CHAPTER 90

Long Wave Interaction with Steeply Sloping Structures

Stéphan T. Grilli [1] and Ib A. Svendsen [2], M. ASCE

Abstract : A fully nonlinear model for free surface potential flows is used to analyze the transformation of solitary waves above a mild slope, from intermediate to shallow water (shoaling, overturning), and to study the interaction of these waves with coastal structures located in the shallow area. Computations include wave runup, overturning and reflection form steep slopes or vertical wall, and from a combination of a slope and a submerged breakwater. Results are compared with other numerical, analytical and experimental results. Effects of the submerged breakwater, of making horizontal velocities more uniform over depth and of reducing wave runup on the slope, are further detailed.

Introduction

In this paper, the Boundary Element Model (BEM) for fully nonlinear waves developed by Grilli, *et al.* 1989, is used to analyze the runup and reflection of solitary waves from steep plane slopes and their transformation over a combination of a mild slope and coastal structures (submerged breakwater in front of a steep slope). The model solves two-dimensional free surface flows, in cases where potential flow is a good approximation. Under such conditions, Green's identity makes it possible to transform Laplace's equation into a Boundary Integral Equation (BIE). Instantaneous solution to this equation is then updated in time using the fully nonlinear kinematic and dynamic boundary conditions at the free surface. Along solid boundaries, no-flow conditions or conditions for generating or radiating waves can be imposed as well.

This approach to nonlinear wave flows has been very successful over the last decade. Particularly noteworthy for important steps in its development are contributions by Longuet-Higgins & Cokelet 1976, Vinje & Brevig 1981 and Dold & Peregrine 1986. Most of the applications so far, however, solved the problem in a transformed space or used complex variable formulations, and introduced the assumption that waves are periodic in space.

[1]Visiting Research Faculty, *Center for Applied Coastal Research*, Department of Civil Engineering, University of Delaware, Newark-DE 19716, USA, Ph.Nb.: 302-4516383

[2]Professor and Chairman (same address)

In our model, the equations are solved directly in the physical space (i.e., without any mapping). This yields a method which is capable of directly adapting to almost any geometry of the boundaries and to periodic as well as non-periodic wave conditions. The BIE is solved using a higher-order Boundary Element Method (first introduced by Brebbia 1978), and the time integration is explicit and of second-order accuracy in time, based on the method of Dold & Peregrine 1986. In the model, wave generation can be done by a wavemaker, by internal sources, or by imposing the potential on the free surface (see Grilli & Svendsen 1989b, 1990). In the present paper, only the numerical wavemaker is presented and used to generate solitary waves.

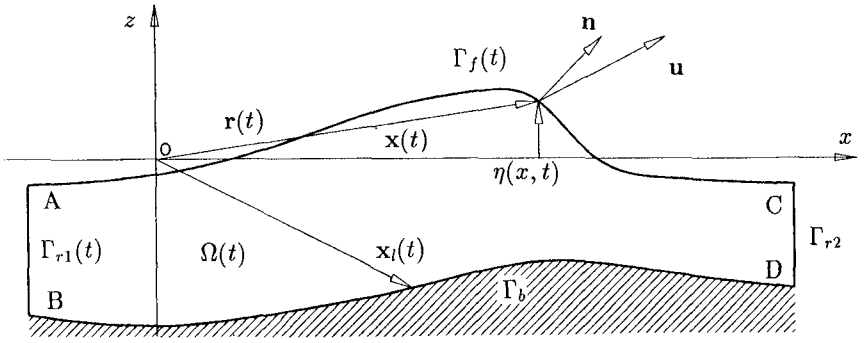

Figure 1: Sketch of the region used in the numerical computations. Definition of geometrical parameters.

Mathematical formulation

Governing equations.– We consider an inviscid irrotational 2-D flow described by a velocity potential $\phi(\mathbf{x},t)$, and the velocity field is given by $\mathbf{u} = \nabla\phi = (u,w)$. Thus, the continuity equation in the fluid domain $\Omega(t)$ with the boundary $\Gamma(t)$ becomes a Laplace equation for ϕ (Figure 1),

$$\nabla^2\phi = 0 \qquad \text{in } \Omega(t) \tag{1}$$

Using the free space Green's function $G(\mathbf{x},\mathbf{x}_l) = -\frac{1}{2\pi}\log|\,\mathbf{x}-\mathbf{x}_l\,|$, (1) becomes the Boundary Integral Equation (BIE),

$$\alpha(\mathbf{x}_l)\phi(\mathbf{x}_l) = \int_{\Gamma(\mathbf{x})}[\frac{\partial\phi}{\partial n}(\mathbf{x})G(\mathbf{x},\mathbf{x}_l) - \phi(\mathbf{x})\frac{\partial G(\mathbf{x},\mathbf{x}_l)}{\partial n}]\,d\Gamma(\mathbf{x}) \tag{2}$$

where $\mathbf{x} = (x,z)$ and $\mathbf{x}_l = (x_l,z_l)$ are position vectors for points on the boundary, $\mathbf{n}$ is the unit outward normal vector. and $\alpha(\mathbf{x}_l)$ is a geometric coefficient.

On the free surface $\Gamma_f(t)$, ϕ satisfies the kinematic and dynamic boundary conditions,

$$\frac{D\mathbf{r}}{Dt} = (\frac{\partial}{\partial t} + \mathbf{u}\cdot\nabla)\mathbf{r} = \mathbf{u} = \nabla\phi \qquad \text{on } \Gamma_f(t) \tag{3}$$

$$\frac{D\phi}{Dt} = -gz + \frac{1}{2}|\nabla\phi|^2 - \frac{p_a - p_o}{\rho} \qquad \text{on } \Gamma_f(t) \tag{4}$$

with $\mathbf{r}$, the position vector of a free surface fluid particle, g the acceleration due to gravity, z the vertical coordinate (positive upwards and $z = 0$ at the undisturbed free surface), p_a the pressure at the surface, p_o a reference pressure (e.g. at infinity) and ρ the fluid density.

General boundary conditions.— In the present applications waves are generated by simulating a plane wavemaker motion on the boundary $\Gamma_{r1}(t)$. In this case, the motion and normal velocity are specified over the paddle by,

$$\nabla\phi \cdot \mathbf{n} \equiv \overline{\frac{\partial\phi}{\partial n}} = \mathbf{u}_p(\mathbf{x}_p(t), t) \cdot \mathbf{n} \qquad \text{on } \Gamma_{r1}(t) \tag{5}$$

where the overline denotes a specified value, and $(\mathbf{x}_p, \mathbf{u}_p)$ are prescribed wavemaker motion and velocity respectively. Along the stationary bottom Γ_b and the tank extremity Γ_{r2} representing a fixed structure (not necessarily vertical as in Figure 1), we have,

$$\nabla\phi \cdot \mathbf{n} \equiv \overline{\frac{\partial\phi}{\partial n}} = 0 \qquad \text{on } \Gamma_b \text{ and } \Gamma_{r2} \tag{6}$$

Time stepping method.— The time stepping, described in detail in Grilli, *et al.* 1989, follows the Eulerian -Lagrangian approach used by Dold & Peregrine 1986. It consists of integrating the two nonlinear free surface conditions (3) and (4) at time t, to establish both the new position of the free surface $\Gamma_f(t)$ and the relevant boundary conditions of Laplace's problems at the next time step $t + \Delta t$. It uses Taylor expansions in terms of the Lagrangian time derivative (as defined in (3)) and the small time increment Δt, for both the position $\mathbf{r}(t)$ and the potential $\phi(t)$ on the free surface, which corresponds to following in time the pathline of a fluid particle, identical to a node of the discretization used for solving the BIE (2). We have so far limited the series to second order in Δt, which requires solving two Laplace problems at each time step (for ϕ and $\frac{\partial\phi}{\partial t}$), to get the coefficients in the series.

After solving a first Laplace problem for $(\phi, \frac{\partial\phi}{\partial n})$ at time t, boundary conditions of a second problem for $(\frac{\partial\phi}{\partial t}, \frac{\partial^2\phi}{\partial t\partial n})$ are determined. Along the free surface, Bernoulli's equation yields,

$$\overline{\frac{\partial\phi}{\partial t}} = -gz - \frac{1}{2}|\nabla\phi|^2 - \frac{p_a - p_o}{\rho} \qquad \text{on } \Gamma_f(t) \tag{7}$$

and along the fixed boundaries, we get,

$$\overline{\frac{\partial^2\phi}{\partial t\partial n}} = 0 \qquad \text{on } \Gamma_b \text{ and } \Gamma_{r2} \tag{8}$$

For a plane wavemaker, we have,

$$\overline{\frac{\partial^2\phi}{\partial t\partial n}} = [\frac{d\,(\mathbf{u}_p\cdot\mathbf{n})}{d\,t} - \mathbf{u}_p\cdot\nabla(\mathbf{u}_p\cdot\mathbf{n})] \qquad \text{on } \Gamma_{r1}(t) \tag{9}$$

Boundary conditions for a plane wavemaker.— Development of (9) for a rigid body motion, with translation α and rotation θ yields (Cointe 1989),

$$\overline{\frac{\partial^2\phi}{\partial t\partial n}} = (\ddot{\alpha}\cdot\mathbf{n}) + \dot{\theta}[(\dot{\alpha}\cdot\mathbf{s}) - \frac{\partial\phi}{\partial s}] - \frac{\partial^2\phi}{\partial n\partial s}(\dot{\alpha}\cdot\mathbf{s}) + \frac{\partial^2\phi}{\partial s^2}(\dot{\alpha}\cdot\mathbf{n}) \tag{10}$$

where the dots denote time derivatives ($\frac{d}{dt}$) following the body motion.

A *piston wavemaker* represents a flat vertical plate moving with horizontal displacement $x_p(t)$ and velocity $u_p(x_p(t),t) = \dot{x}_p(t)$. Hence from (5),(10), the boundary conditions read after some calculations,

$$\overline{\frac{\partial\phi}{\partial n}} = -u_p, \qquad \overline{\frac{\partial^2\phi}{\partial t\partial n}} = -\dot{u}_p - u_p\frac{\partial^2\phi}{\partial s^2} \qquad \text{on } \Gamma_{r1}(t) \tag{11}$$

A *Flap wavemaker* corresponds to a flat plate, hinged at the bottom at $\mathbf{x}_g = (0,-d)$ and rotating an angle $\theta(t) \in [\frac{\pi}{2},0]$ (negative clockwise). We define $x_p(t)$ and $u_p(x_p(t),t) = \dot{x}_p(t)$, the flap horizontal displacement and velocity respectively at the undisturbed free surface $z = 0$. Hence, from (5),(10), the boundary conditions read after some calculations,

$$\overline{\frac{\partial\phi}{\partial n}} = r_g\dot{\theta}, \qquad \overline{\frac{\partial^2\phi}{\partial t\partial n}} = r_g\,\ddot{\theta} + \dot{\theta}\,(r_g\frac{\partial^2\phi}{\partial s^2} - \frac{\partial\phi}{\partial s}) \qquad \text{on } \Gamma_{r1}(t)$$

$$\dot{\theta} = -R\,u_p, \qquad \ddot{\theta} = -R\,[\dot{u}_p - 2\,u_p^2\frac{x_p}{d}], \qquad r_g = R\sqrt{d^2+x_p^2}\,[\alpha\frac{x_p}{d} + \beta + d] \tag{12}$$

where $R = d/(d^2+x_p^2)$, and (α,β) represent points along the flap.

Numerical implementation

The BIE (2), equivalent to the Laplace's problems (1) for ϕ and the equivalent BIE problem for $\frac{\partial\phi}{\partial t}$, is solved by a Boundary Element Method (BEM, Brebbia 1978) using a set of collocation nodes on the boundary and higher-order elements to interpolate between the collocation nodes. Quasi-spline elements (Longuet-Higgins & Cokelet 1976) are used on the free surface, and isoparametric elements elsewhere (linear to quartic).

Each integral in (2) is transformed into a sum of integrals over each boundary element. Non-singular integrals are calculated by standard Gauss quadrature rules. A kernel transformation is applied to the weakly singular integrals, which are then integrated by a numerical quadrature exact for the logarithmic singularity. An adaptive numerical integration is used for improving the accuracy of the regular integrations near corners (A-D, Fig. 1) and other places, like the overturning jet in breakers (as, e.g., in Fig. 8c,d), where elements on different parts of the boundary get close to each other.

Details of the numerical implementation can be found in Grilli, *et al.* 1989,1989b,1990, along with a discussion of problems associated with surface piercing bodies, such as wavemakers.

Generation of a solitary wave

By a piston wavemaker.—In the following, primes denote dimensionless variables : lengths are non-dimensio- nalized by d, times by $\sqrt{\frac{d}{g}}$, velocities by $\sqrt{gd}$ and accelerations by g.

For a wave of permanent form, Goring 1978 determined to the first-order, the motion required by a piston wavemaker to generate a specified water surface elevation η immediately in front of the wavemaker (see Grilli & Svendsen 1989a, for detail) as,

$$x_p(t) = \int_0^t \frac{c\,\eta(x,\tau)}{d+\eta(x,\tau)}\,\mathrm{d}\tau \tag{13}$$

A *first-order* solitary wave profile of amplitude H' in water of constant depth $d' = 1$ is given by,

$$\eta'(x',t') = H'\mathrm{sech}^2[\kappa(x'-c't')] \tag{14}$$

where $\kappa = \frac{\sqrt{3H'}}{2}$ and the celerity $c' = \sqrt{1+H'}$. Substituting (14) into (13) with $x' = x'_p(\tau')$ required throughout the integration gives the piston motion. The profile (14), however, is truncated at a distance $x' = \lambda'$ from the origin, before it is used in the computations. Setting $x' = x'_p + \lambda'$ in (14) and integrating (13) we get $x'_p(t')$ and, by derivation, $u'_p(t')$ and $\dot{u}'_p(t')$ (see Grilli & Svendsen 1990, for the complete expressions), which, introduced into (11), define the boundary conditions at the wavemaker.

Solitary waves of small amplitude ($H' < 0.2$) are well generated by this method. For such waves, the *first-order* profile (14) is indeed quite close to the exact solution. For steep waves ($H' \geq 0.2$), however, due to nonlinear effects, solitary waves generated by the piston adjust their shape as they propagate, and shed a tail of oscillation behind them (Grilli & Svendsen 1989a). In fact, this was already observed by Goring 1978, in his experiments.

Numerically exact solitary waves.—Solitary waves which are as close to being exact as the discretization allows –"numerically exact waves"– are also used in the computations. They are computed using the method developped by Tanaka 1986, and established as initial condition in the constant depth part of the computational domain.

Reflection from a vertical wall

Reflection of solitary waves from a vertical wall has been used to validate the numerical model, and to compare results with other numerical, analytical or experimental results. In this application, numerically exact solitary waves have also

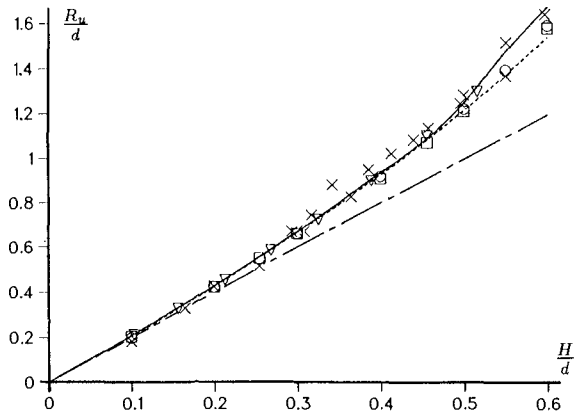

Figure 2: Maximum runup $\frac{R_u}{d}$ for reflection from a vertical wall of solitary waves of height $\frac{H}{d}$. Results of : (——) spline fitting to BEM for the *exact* waves, (□) BEM for the *first-order* waves, (○) Chan & Street 1970 Euler eq., (▽) Fenton & Rienecker 1982 Fourier Method, (×) Camfield & Street 1969 exper., (- - - -) Su & Mirie (1980) 3rd-order analytical solution and (— - —) linear solution.

been used along with the approximate waves generated by the piston wavemaker.

Runup.—In Figure 2, maximum runup values $\frac{R_u}{d}$ obtained with the BEM model for the exact and the approximate (1st-order) waves, are compared with a finite difference solution of Euler equations by Chan & Street 1970 (CH&S), a higher-order Fourier solution by Fenton & Rienecker 1982 (F&R), experimental results by Camfield & Street 1969 (CA&S), and a 3rd-order analytical solution by Su & Mirie 1980 (S&M). One sees that, up till about $\frac{H}{d}$=0.45, all theoretical methods predict similar runups. Above that value, the 3rd-order theory predicts smaller runups, implying that contributions of order higher than third are becoming important. For high waves, F&R's solution coincides closely with our results for the exact waves, and CH&S's solution agrees well with those of our 1st-order waves. This is likely due to the approximate way CH&S generated their initial waves, which makes them qualitatively closer to waves generated by a wavemaker. Finally, CA&S's experiments agree well with the higher-order results.

Pressure force.—Once the BEM solution for the wave motion has been computed, essentially all details of the flow pattern are known, including pressures. We can therefore also calculate the forces and moments exerted on the structure. We found that maximum forces and moments predicted by the BEM closely correspond to F&R and S&M results, up till $\frac{H}{d}$=0.5. For higher waves, a somewhat surprising result of the BEM is a double maximum found in the time variation of the force and moment (Figure 3).

Reflected wave.—A detailed analysis of the reflected waves shows that an os-

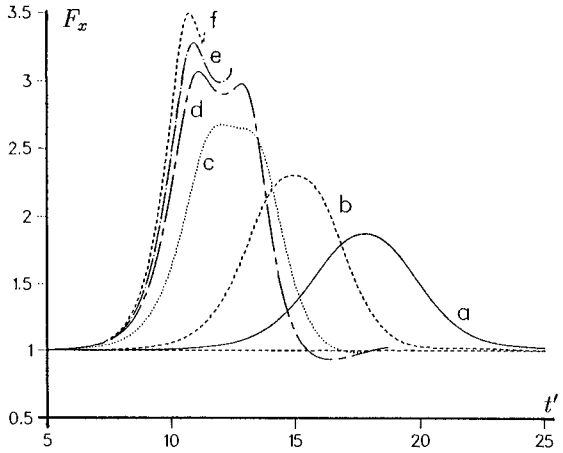

Figure 3: Development in time of total dimensionless pressure force F_x on a vertical wall during reflection of an *exact* solitary wave. $\frac{H}{d}$: (a) 0.2, (b) 0.3, (c) 0.4, (d) 0.5, (e) 0.55, (f) 0.6.

cillatory tail is created by the reflection process, along with negative rundown values on the wall (of about 10% $\frac{H}{d}$ for $\frac{H}{d}$=0.5). Energy is transmitted from the main leading wave to the tail, which results in a slight decrease in wave amplitude after reflection (of about 10% $\frac{H}{d}$ for $\frac{H}{d}$=0.5). These observations tie well in with the 5th-order analytical results by Byatt-Smith 1988. Right after reflection, the reflected wave is also found slightly faster than the incident wave, even though it is smaller (by about 0.5% for $\frac{H}{d}$=0.5). This is due to highly transient changes in shape, energy partition and celerity of the wave, which take place over large propagation distances.

Reflection from a steep slope

Reflection from steep slopes (45° and 70°) has been examined for solitary waves generated by a piston wavemaker, the same way as in the laboratory experiments by Losada, *et al.* 1986 (LVN). Comparison with the measurements shows that phenomena such as generation, propagation and runup on a steep slope of large amplitude waves can be accurately predicted by our model. Even small scale oscillations in the experiments (like the oscillatory tail after reflection) are reproduced quite accurately. An example is given below.

Runup and rundown.—Reflection is computed on both the 45° and 70° slopes for waves of $\frac{H}{d} \simeq 0.26, 0.45$. Results show maximum runup values $\frac{R_u}{d}$ are in good agreement with LVN's experiments (within 2.5% for $\theta = 45°$ and 2.0% for $\theta = 70°$). The agreement for the rundown figures $\frac{R_d}{d}$ is somewhat less good but it should be noted that LVN found this quantity quite difficult to measure. Details

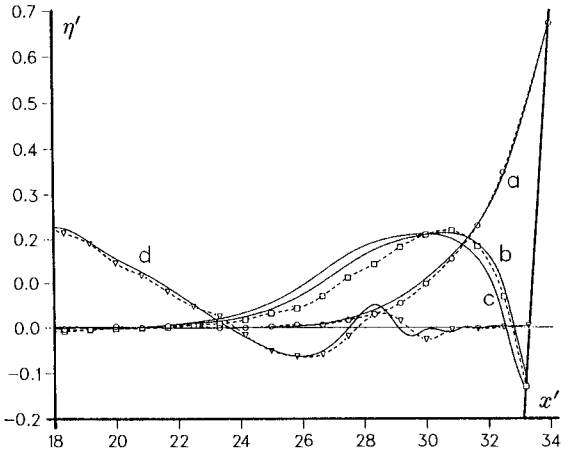

Figure 4: Comparison between computations (——) and measurements (- - -) by Losada, *et al.* 1986 for reflection from a 45° slope of a solitary wave of $\frac{H}{d}$= 0.269. The symbols mark data points and the dotted curve is a spline fit to these points. (a) Instant of maximum runup. (b) 0.44 time unit before rundown. (c) Instant of lowest position of water surface. (d) Back of the reflected wave.

can be found in Grilli & Svendsen 1989a.

Free surface elevation.—Figure 4 shows results for the reflection of a wave of $\frac{H}{d}$=0.269 from a 45° slope. The computations are compared with the surface profiles measured by LVN at three different times, of which the first available is the instant of maximum runup (curves a) used for synchronization. In general, the agreement is considered good. Results, however, do not quite coincide at the time of rundown (curve c). The agreement is somewhat better with a profile computed at a time slightly before the instant of rundown (curve b). This shows that, as pointed out by LVN, both rundown and instant of rundown are quite difficult to measure since the surface motion along the slope is important over a very short time (the whole rundown process only lasts a small fraction of a second in the experiments).

Internal velocities.—Motivated by the accuracy of the computations the method has also been used to analyze flow properties such as velocity and pressure fields that have not been measured during the experiments. Water particle velocities have been computed above 30° and 45° slopes, during runup-rundown of a wave of $\frac{H}{d}$=0.46. Figure 5 shows quite complex flows above a 30° slope, with jet-like details (Fig. 5a,b) and a stagnation point (Fig. 5b) climbing up the slope during runup. It is found, the flow is never completely at rest at any moment of the wave reflection (even at the instant of runup in Fig. 5c). Finally, Figure 5d shows the initiation of breaking during the rundown process (backwash), at the rearside of

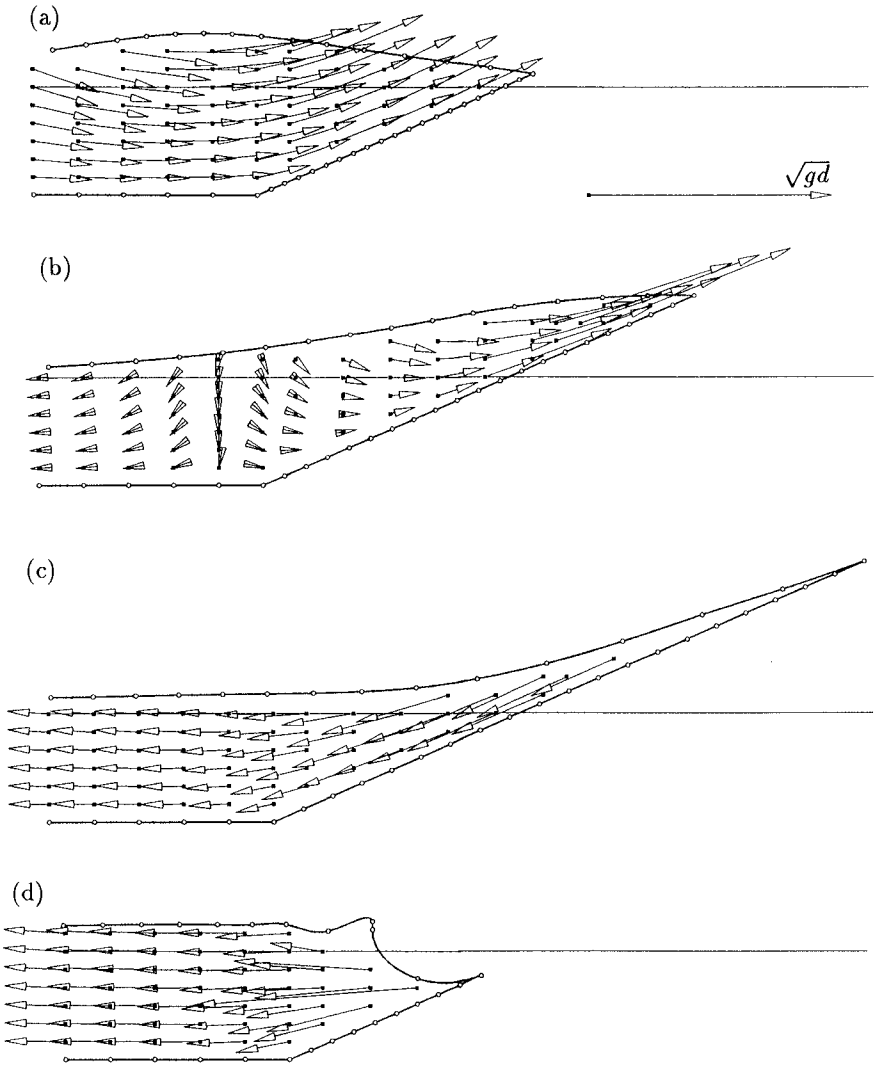

Figure 5: The internal velocity field during runup of a first-order solitary wave with $\frac{H}{d}$= 0.46 on a 30° slope, at time $t' - t'_a$ = (a) : 0, (b) : 0.40, (c) : 0.95 (maximum runup), (d) : 1.90.

and in the direction oposite to the propagation of the reflected wave.

Detailed analysis of the results (Svendsen & Grilli 1990) shows that, for both slopes, horizontal velocities are significantly non-uniform over the depth (with variations of 25-35%) and that, accordingly, important non-hydrostatic pressures are generated (up to 80% on a 45° slope and 180 % on a 30° slope). This invalidates the assumptions underlying the Nonlinear Shallow Water equations and makes their use questionable in these situations. The maximum runup, however, is found to compare reasonably well with the analytical results obtained by, e.g., Synolakis (1987) using those approximate equations.

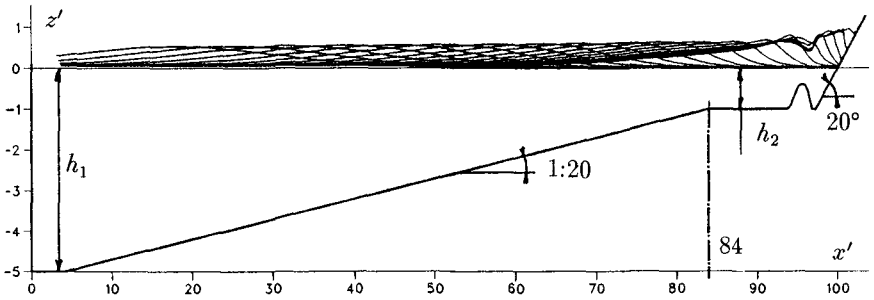

Figure 6: Sketch of composite domain : The shoaling zone is defined for $x' \leq 84$, and the shallow zone for $x' > 84$. Solitary waves are generated by a piston wavemaker at the leftward boundary.

Shoaling and reflection over a complex geometry

Solitary waves are propagated from deep to shallow water, in a domain with the bottom configuration of Figure 6. Waves of $\frac{H_1}{h_1} = 0.05$ to 0.2 are generated by a piston wavemaker, at the left hand boundary, in water of depth $h_1 = 5$, and are propagated over a mild 1:20 slope towards a region of depth $h_2 = 1$. At the extremity of this region, there is a combination of a submerged breakwater and a 20° slope. The length of the domain is $100h_2$, and the regions with $x' = \frac{x}{h_2} < 84$ (the end of the mild slope), or > 84 are named the shoaling and the shallow zones, respectively.

Shoaling zone.—Shoaling of waves of $\frac{H_1}{h_1}$=0.05,0.10,0.15 and 0.2 has been computed. In a logarithmic scale, results in Figure 7 show that, for $-\log\left(\frac{h}{h_1}\right) \leq 0.45$ (i.e., $x' \simeq 60$), the rate of shoaling is close to, but not quite, the one predicted by Green's law. The average slope of the 4 curves in Figure 7 actually is closer to 1:5 in this region. During shoaling, incident waves reflect on the 1:20 slope. Due to the finite length of the computational domain, however, reflected waves propagating backward in the domain also reflect on the wavemaker. This leads to a slight increase in water level in the shoaling zone. Since smaller solitary waves are longer, the relative increase in level is somewhat more pronounced for

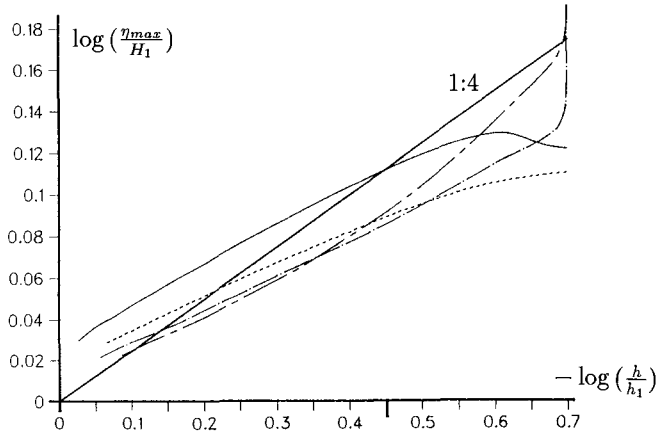

Figure 7: Maximum wave amplitude $\frac{\eta_{max}}{H_1}$ in shoaling zone, as a function of relative depth $\frac{h}{h_1}$ for $\frac{H_1}{h_1}$: (——) 0.05, (- - -) 0.10, (–.–.) 0.15, (— –) 0.20. The straight line represents theoretical Green's law : $\frac{\eta_{max}}{H_1} \propto (\frac{h}{h_1})^{-\frac{1}{4}}$

the smallest waves. This is illustrated by the vertical shifts between the curves in Figure 7.

Further up the slope, for $-\log(\frac{h}{h_1}) > 0.45$ (i.e., $x > 60$), the rate of shoaling of the two smallest waves reduces, whereas the two largest waves shoal up even more and at an increasing rate. This is likely because the smallest waves, being longer, start earlier feeling the influence of the shallow water zone ($h = h_2$).

Shallow zone.—Figure 8c and d show that the largest waves of initial height $\frac{H_1}{h_1} = 0.15$ and 0.20 continue shoaling in the shallow zone, even though it is of constant depth. Their profile becomes more and more asymmetric, and their amplitude peaks up to $\frac{\eta_{max}}{h_2} \simeq 1.4$ and 1.6. They eventually become plunging breakers, somewhat before reaching the submerged breakwater. Hence, this shows, highly transient waves can reach breaking heights of more than twice the classical 0.78 times the local depth.

The two smallest waves of $\frac{H_1}{h_1} = 0.05$ and 0.1 (Figure 8a and b) shoal up to $\frac{\eta_{max}}{h_2} \simeq 0.55$ and 0.80 (at $x' \simeq 95$), respectively, propagate over the submerged breakwater and run on the slope up to heights of $\frac{R_u}{h_2} \simeq 0.90$ and 1.5 respectively. Even higher relative heights of $\frac{\eta_{max}}{h} = 1.26$ and 1.66 respectively, are locally reached above the submerged breakwater.

Figure 8b also shows the wave of $\frac{H_1}{h_1} = 0.1$, eventually, is similar to a collapsing breaker. Computations of internal velocities above the slope, for a time slightly before the collapsing, show that velocities are close to being uniform over the depth. This is unlike the results obtained (e.g., in Fig. 5) for wave runup on steep slopes without a submerged breakwater at their toe, where the non-uniformity of the horizontal velocity was as high as 35%. Computations

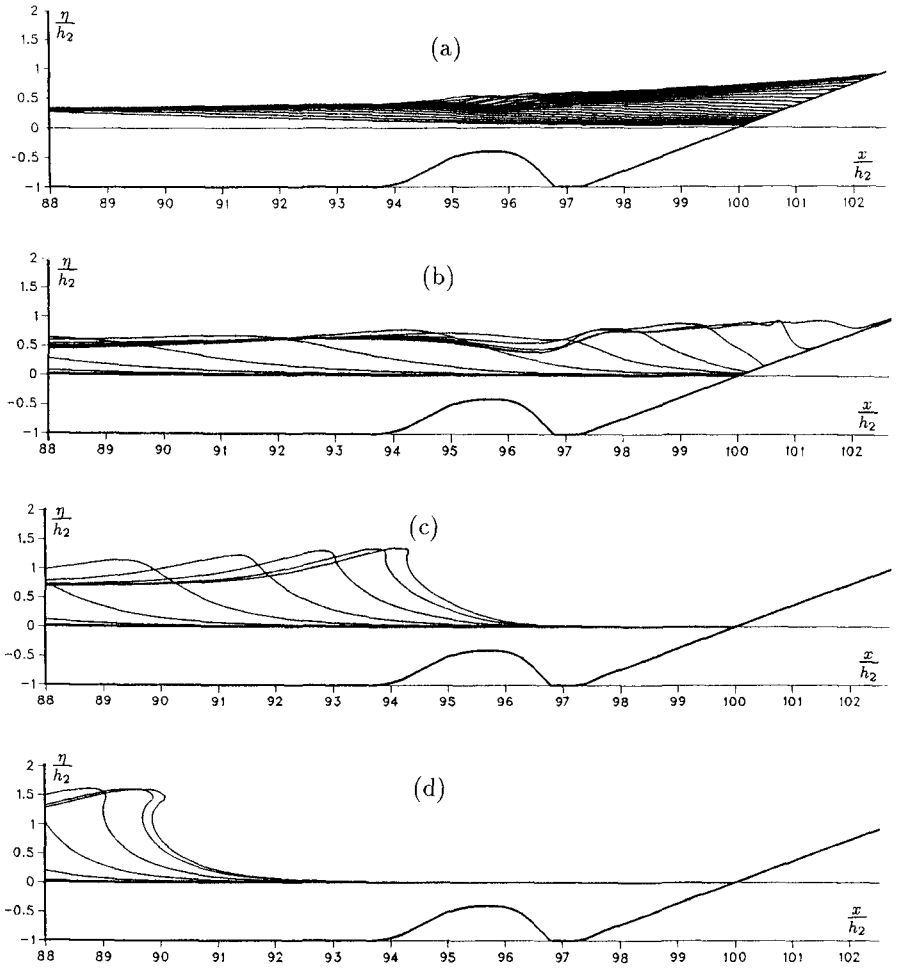

Figure 8: Free surface elevation $\frac{\eta(x)}{h_2}$ in the shallow zone for $\frac{H_1}{h_1}$: (a) 0.05, (b) 0.10, (c) 0.15, (d) 0.20. Profiles are plotted each 10 (varying) time steps.

made in the same domain, for the same wave as in Figure 8b, but without the submerged breakwater, give a maximum runup of more than twice the previous result ($\frac{R_u}{h_2} = 3.16$). This shows, the submerged breakwater has the effect, not only of making velocities more uniform (i.e., decreasing the maximum velocity), but also of reducing wave runup. Both these effects mean reduction of wave action on the steep slope.

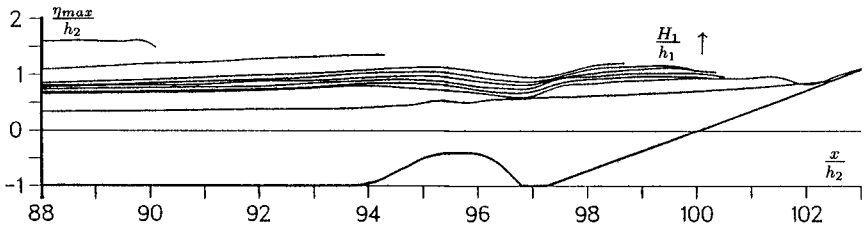

Figure 9: Envelope of maximum surface elevation $\frac{\eta_{max}}{h_2}$ in the shallow zone : curves represent, from down to up, $\frac{H_1}{h_1}$: 0.05, 0.10, 0.105, 0.110, 0.115, 0.120, 0.125, 0.15, 0.20.

In order further to analyze the transition between situation (b) and (c) in Figure 8, computations have also been made for intermediate wave heights of $\frac{H_1}{h_1} = 0.105$, 0.110, 0.115, 0.120 and 0.125. Figure 9 shows envelopes of the water elevations $\frac{\eta_{max}}{h_2}$ obtained for these waves, as well as for the waves used in Figure 8. When wave height is slightly increased above $\frac{H_1}{h_1} = 0.1$, results show, the breaking type changes from collapsing to surging and plunging. At the same time, the breaking point (i.e., the abscissa of the maximum amplitude of the last computed profile) moves slightly backward on the slope and the breaking height becomes slightly larger. For all waves, there is a trough in the envelope, slightly downstream of the submerged breakwater, corresponding to where velocities are becoming more uniform. Further downstream, about at the toe of the slope, wave height is building up again. This process corresponds to the transformation of kinetic energy into potential energy and seems to occur, here, at a faster rate than in the situation without the submerged breakwater. Hence, wave height builds up more and over a larger area above the slope, and runup values are reduced.

References

Brebbia, C.A. (1978) *The Boundary Element Method for Engineers.* John Wiley & Sons, U.K..

Camfield, F.E. & Street, R.L. (1969) "Shoaling of Solitary Waves on Small Slopes." *ASCE,* **WW95,** 1-22.

Chan, R.K. & Street, R.L. (1970) "A Computer Study of Finite-amplitude Water Waves." *J. Comp. Phys.* **6** 68-94.

Cointe, R. (1989) "Quelques aspects de la simulation numérique d'un canal à houle." *Thèse de Docteur de l'Ecole Nationale des Ponts et Chaussées,* 284 pps.

Dold, J.W. & Peregrine, D.H. (1986) "An Efficient Boundary Integral Method for Steep Unsteady water Waves." *Numerical methods for Fluid Dynamics II* (ed. K.W. Morton & M.J. Baines), pp. 671-679. Clarendon Press, Oxford.

Fenton J.D. & Rienecker, M.M. (1982) "A Fourier Method for Solving Nonlinear Water-Wave Problems : Application to Solitary-Wave Interactions." *J. Fluid Mech.* **118,** 411-443.

Goring D.G. (1978) "Tsunamis - The Propagation of Long Waves onto a Shelf." *W.M. Keck Laboratory of Hydraulics and Water Ressources, California Institute of Technology, Report No.* **KH-R-38.**

Grilli, S., Skourup, J. & Svendsen, I.A. (1989) "An Efficient Boundary Element Method for Nonlinear Water Waves." *Engineering Analysis with Boundary Elements,* **6** (2), 97-107.

Grilli, S. & Svendsen, I.A. (1989a) "Computation of Nonlinear Wave Kinematics during Propagation and Runup on a Slope." In *Water Wave Kinematics* (Proc. NATO ARW, Molde, Norway, May 89) (ed. A. Torum & O.T. Gudmestad), NATO ASI Series E: Applied Sciences Vol. **178,** 387-412. Klüwer Academic Publishers.

Grilli, S. & Svendsen, I.A. (1989b) "The Modelling of Highly Nonlinear Waves : Some Improvements to the Numerical Wave Tank." In *Advances in Boundary Elements (Proc. 11th Intl. Conf. on Boundary Elements, Cambridge-Massachusetts, USA, August 89),* Vol. 2 (ed. C.A. Brebbia & J.J. Connor), pp. 269-281. Computational Mechanics Publication. Springer-Verlag, Berlin.

Grilli, S. & Svendsen, I.A. (1990) "Corner Problems and Global Accuracy in the Boundary Element Solution of Nonlinear Wave Flows." *Engineering Analysis with Boundary Elements* **7** (4) (in press).

Longuet-Higgins, M.S. & Cokelet, E.D. (1976) "The Deformation of Steep Surface Waves on Water - I. A Numerical Method of Computation." *Proc. R. Soc. Lond.* **A350,** 1-26.

Losada, M.A., Vidal, C. & Nunez, J. (1986) "Sobre El Comportamiento de Ondas Propagádose por Perfiles de Playa en Barra y Diques Sumergidos." *Dirección General dc Pucrtos y Costas Programa de Clima Maritimo. Universidad de Cantábria. Publicación No.* **16.**

Su, C.H. & Mirie, R.M. (1980) "On Head-on Collisions between two Solitary Waves." *J. Fluid Mech.* **98** 509-525.

Svendsen, I.A. & Grilli, S. (1990) "Nonlinear Waves on Steep Slopes." *J. Coastal Research* **SI 7,** 185-202.

Synolakis, C.E. (1987) "The Runup of Solitary Waves." *J. Fluid Mech.* **185,** 523-545.

Tanaka, M. (1986) "The Stability of Solitary Waves." *Phys. Fluids* **29** (3), 650-655.

Vinje, T. & Brevig, P. (1981) "Numerical Simulation of Breaking Waves." *Adv. Water Resources* **4,** 77-82.